Quantized perfect transmission in graphene nanoribbons with random hollow adsorbates

Jia-Le Yu [1], Zhe Hou,[2] Irfan Hussain Bhat [1], Pei-Jia Hu [1], Jia-Wen Sun,[1]
Xiao-Feng Chen,[1,3] Ai-Min Guo [1,*] and Qing-Feng Sun [4,5]

[1]*Hunan Key Laboratory for Super-microstructure and Ultrafast Process, School of Physics,*
Central South University, Changsha 410083, China
[2]*School of Physics and Technology, Nanjing Normal University, Nanjing 210023, China*
[3]*School of Physical Science and Technology, Lanzhou University, Lanzhou 730000, China*
[4]*International Center for Quantum Materials, School of Physics, Peking University, Beijing 100871, China*
[5]*Hefei National Laboratory, Hefei 230088, China*

Impurities exist inevitably in two-dimensional materials as they spontaneously adsorb onto the surface during fabrication, usually exerting detrimental effects on electronic transport. Here, we focus on a special type of impurities that preferentially adsorb onto the hollow regions of graphene nanoribbons (GNRs), and study how they affect the quantum transport in GNRs. Contrary to previous knowledge that random adatoms should localize electrons, the so-called Anderson localization, noteworthy quantized conductance peaks (QCPs) are observed at specific electron energies. These QCPs are remarkably robust against variations in system size, GNR edge, and adatom properties, and they can reappear at identical energies following an arithmetic sequence of device width. Further investigation of the wave function reveals a unique transport mode at each QCP energy which transmits through disordered GNRs reflectionlessly, while all the others become fully Anderson localized, indicating the survival of quantum ballistic transport in the localized regime. Our findings highlight the potential utility of hollow adatoms as a powerful tool to manipulate the conductivity of GNRs, and deepen the understanding of the interplay between impurities and graphene.

I. INTRODUCTION

As impurities exist inevitably in two-dimensional materials, the subject on how they affect the electronic transport properties of graphene has been attracting extensive and ongoing interest [1–11]. In the presence of long-ranged impurities, graphene maintains high mobility due to Klein tunneling [12–17], but it experiences Anderson localization with short-ranged random impurities when the intervalley scattering is strong [18–22]. It has been further demonstrated that the electronic properties of graphene can be significantly altered by simply manipulating the distribution and type of adatoms when adhering to graphene's surface [23–30]. In general, adatoms adhere to graphene at three different locations [21,31–36]: top sites (atop carbon atoms), bridge sites (between two adjacent carbon atoms), and hollow sites (at the center of hexagons). Adatoms at the top sites have been demonstrated to induce band gaps [37–40], and those at the bridge sites are known to induce magnetic moments [41–43]. Adatoms occupying hollow sites are usually associated with heavy adatoms [44–51] [see the yellow balls in Fig. 1(a)], which have been shown to induce more intriguing and versatile quantum phases in graphene, such as the spin Hall effect [50–53], topological insulators [32,54,55], and even superconductivity [56–59]. However, the impact of hollow adatoms on

graphene's properties, particularly the quantum transport, has rarely been explored to date.

In this paper, we study theoretically the electron transport through a two-terminal graphene nanoribbon (GNR) with randomly distributed hollow adatoms, as depicted in Fig. 1(a). Although the overall electron transmission is dramatically reduced, a number of quantized conductance peaks (QCPs) with the value $2e^2/h$ emerge at specific electron energies. These QCPs remain unchanged by varying nanoribbon lengths and edges, adatom properties, and more importantly they persist in the Anderson localization regime at high adatom concentrations. Furthermore, identical QCPs are observed for various nanoribbon widths, which follow the arithmetic progression rule. By analyzing the wave function of carbon atoms in each hexagon, the QCPs can be understood rather simply from the renormalized Schrödinger equation. That is, when the sum of the wave function of the six carbon atoms in each hexagon is exactly zero at these QCP energies, the influence of adatoms negates, thus making the transmission ballistic. These results unravel the coexistence of two extreme quantum transport phenomena, quantized ballistic transport and Anderson localization, on the same platform, and may facilitate designing graphene devices based on impurities instead of their detrimental effects.

The rest of the paper is organized as follows. Section II introduces the model Hamiltonian of graphene with randomly distributed adatoms at the hollow sites, and the Green's function to calculate the conductance. Sections III–V display the
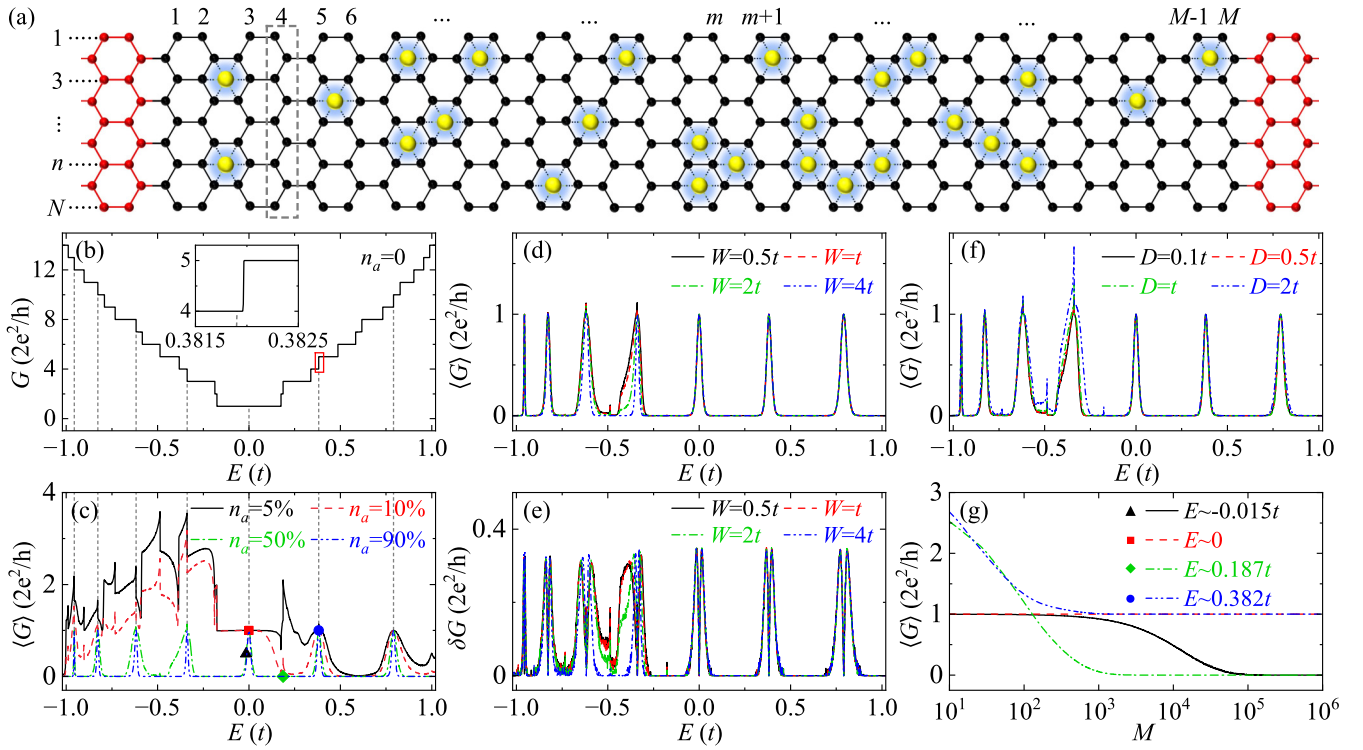
FIG. 1. Structure and electron transport property of disordered armchair GNRs. (a) Schematic of a disordered GNR device coupled to left and right semi-infinite GNRs. Here, the black and red balls denote carbon atoms, and the yellow ones are adatoms situated randomly at the hollow regions. The device size is described by the number of slices, M, and the number of carbon atoms in each slice, N, as indicated by the rectangle. (b) Energy-dependent conductance G of the pristine GNR, with the inset showing the magnified view in the rectangle. Energy-dependent averaged conductance $\langle G \rangle$ of disordered GNRs for (c) several adatom concentrations n_a, (d) different on-site energy disorder strengths W, and (f) different bond disorder strengths D. (e) Standard deviation δG referring to (d). (g) $\langle G \rangle$ vs length M at the energies marked by different symbols in (c). The parameters are $N = 29$, $M = 10^4$, $n_a = 50\%$, $\epsilon_\alpha = 0$, and $\gamma_\alpha = t$, unless specified in the figure.

robustness of QCPs, the width-dependent QCPs, and their physical origin, respectively. Finally, the results are summarized in Sec. VI.

II. MODEL AND METHOD

The electron transport through disordered GNRs, with randomly distributed adatoms at the hollow sites, can be described by the tight-binding Hamiltonian:

$$\mathcal{H} = -t \sum_{\langle i,j \rangle} c_i^\dagger c_j + \sum_\alpha \epsilon_\alpha d_\alpha^\dagger d_\alpha + \sum_{\langle \alpha,j \rangle} \gamma_\alpha (d_\alpha^\dagger c_j + c_j^\dagger d_\alpha). \quad (1)$$

Here, $c_i^\dagger$ (c_i) is the creation (annihilation) operator of an electron at site i of the graphene lattice, $\langle i, j \rangle$ denotes all the nearest-neighbor sites with the hopping integral t chosen as the energy unit, and the on-site energy of graphene is taken as the energy reference point. ϵ_α is the on-site energy of an adatom at site α with $d_\alpha^\dagger$ (d_α) the creation (annihilation) operator. The last term denotes the coupling between adatom α and all the nearest-neighbor carbon atoms with γ_α the isotropic hopping integral which only depends on adatoms.

From the Landauer-Büttiker formula [60–65], the conductance of the two-terminal GNR is obtained as $G = (2e^2/h)\mathrm{Tr}[\boldsymbol{\Gamma}_L \mathbf{G}^r \boldsymbol{\Gamma}_R \mathbf{G}^a]$, with $\mathbf{G}^r(E) = [\mathbf{G}^a(E)]^\dagger = [E\mathbf{I} - \mathbf{H}_c - \boldsymbol{\Sigma}_L^r - \boldsymbol{\Sigma}_R^r]^{-1}$ the Green's function, and $\boldsymbol{\Gamma}_{L/R} = i(\boldsymbol{\Sigma}_{L/R}^r - \boldsymbol{\Sigma}_{L/R}^a)$ the linewidth function. Here, E is the

electron energy, $\mathbf{H}_c$ the Hamiltonian of the central scattering region (CSR), and $\boldsymbol{\Sigma}_{L/R}^{r(a)}$ the retarded (advanced) self-energy due to the coupling to the left/right semi-infinite GNR. As the adatoms are characterized by three parameters of ϵ_α, γ_α, and adatom concentration n_a, we consider all possible situations by varying one parameter and fixing the other two, where n_a is defined as the ratio of the number of adatoms to that of hexagons in the CSR. (i) In the case of a different number of adatoms, the adatom concentration is varied, whereas the other two parameters are fixed as $\epsilon_\alpha = 0$ and $\gamma_\alpha = t$, with t the hopping integral of graphene. (ii) In the case of different types of adatoms, we consider the most disordered situation and ϵ_α distributes uniformly in $[-W/2, W/2]$, while the other parameters are set to $n_a = 50\%$ and $\gamma_\alpha = t$. (iii) In the case of different adatom sizes and vertical distances from the graphene plane [66–68], γ_α distributes uniformly within $[t - D/2, t + D/2]$, while the other parameters are set to $n_a = 50\%$ and $\epsilon_\alpha = 0$. Here, W and D are, respectively, the on-site energy and bond disorder strengths. Since the graphene synthesized in experiments is usually very large [69–71], the length of the CSR is taken as $M = 10^4$, which refers to approximately 2.13-μm-long GNRs, and the width is set to $N = 29$. Such long disordered GNRs allow for better exploration of the localization phenomenon and QCPs. The conductance is averaged over $2 \times 10^7/M$ disordered samples,

and the bond current is obtained from a single GNR sample. All these parameters will be used throughout the paper, unless stated otherwise.

III. ROBUSTNESS OF QCPs

We first study the electron transport through armchair GNRs by varying the adatom concentration from $n_a = 0\%$ to 90%, as shown in Figs. 1(b) and 1(c). As compared with the pristine GNR [Fig. 1(b)], the introduction of adatoms results in a dramatic reduction of the electron transmission along disordered GNRs [Fig. 1(c)], and there exist zero conductance plateaus at a high adatom concentration of $n_a = 50\%$ and 90%, a sign of Anderson localization induced by the scattering from randomly distributed adatoms [19,72–75]. In addition, the averaged conductance $\langle G \rangle$ is asymmetric with respect to the line $E = 0$, because the triangle structure arises simultaneously when the adatoms situate at hollow sites and subsequently the electron-hole symmetry is broken [76,77]. Interestingly, several QCPs of conductance quantum emerge at discrete energies distributed within the whole transmission spectrum and locate around the plateau transition points [see the inset of Fig. 1(b)]. This phenomenon is different from perfectly conducting channels observed in disordered GNRs by considering long-ranged impurities [13], which occur exclusively around the Dirac points and the resulting impurity potential varies slowly on the atomic scale. These QCPs exhibit electron-hole asymmetry as well, where at the electron side the QCPs arise for small n_a and at the hole side they only manifest for large n_a. All these phenomena still hold for disordered GNRs with a zigzag edge (see the Supplemental Material [78]), and we will focus on armchair GNRs in the following.

We then investigate how the on-site energy of adatoms and their coupling to the neighboring carbon atoms affect the QCPs. Figures 1(d) and 1(f) show the averaged conductance $\langle G \rangle$ vs E by considering the on-site energy and bond disorder, respectively. We can see that the profile of most QCPs remains the same by changing W or D [Figs. 1(d) and 1(f)]. By contrast, the two QCPs at $E \sim -0.618t$ and $-0.338t$ seem to be sensitive to the adatoms, where $\langle G \rangle$ decreases with increasing W and increases with D. The latter anomalous behavior originates from the fact that, with increasing D, the adatoms will effectively decouple from the GNR and the adatom concentration is declined, leading to the increment of the transmission ability, because of the finite-size effect. Indeed, all these QCPs remain unchanged for sufficiently long GNRs, regardless of the values of W and D, implying the robustness against the adatoms.

Figure 1(e) plots the energy-dependent standard deviation $\delta G \equiv \sqrt{\langle G^2 \rangle - \langle G \rangle^2}$, in accordance with Fig. 1(d). There always exist dips of $\delta G = 0$ at the QCP positions and two deviation peaks of $\delta G \sim 0.66e^2/h$ for each QCP. Indeed, the characteristic of $\delta G = 0$ can hold well at the QCP positions, regardless of the GNR length M and the disorder strengths W and D. This indicates that the QCPs of conductance quantum can always be observed in any single disordered GNR sample, as further confirmed in Figs. 2(a) and 2(b). When the electron energy is far away from the QCP positions, the standard deviation satisfies $\delta G = 0$ [see the electron side in
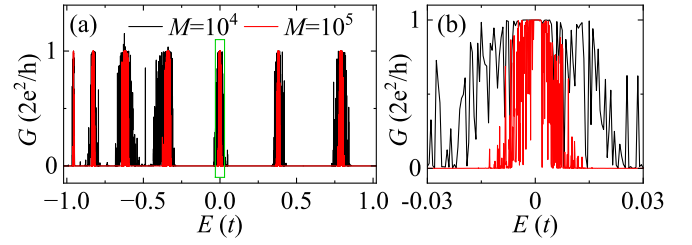
FIG. 2. Electron transport along a single disordered armchair GNR. (a) Energy-dependent conductance G of a single disordered GNR with length being $M = 10^4$ and 10^5, and (b) magnified view in the green rectangle of (a). Here, the on-site energy disorder strength is $W = t$ and the other parameters are the same as in Fig. 1(d).

Fig. 1(e)], indicating the localization behavior in any disordered GNR with length $M = 10^4$. Figure 1(g) displays $\langle G \rangle$ vs M for typical electron energies marked by different symbols in Fig. 1(c). It is clear that, at the QCP positions, $\langle G \rangle$ usually decreases with increasing M and then saturates at conductance quantum in the large length limit [see the red dashed and blue dashed-dotted-dotted lines in Fig. 1(g)], implying the quantum ballistic transport behavior of the QCPs. When E deviates from the QCP positions, $\langle G \rangle$ gradually decreases with increasing M and finally becomes zero, which corresponds to the Anderson localization for non-QCP energies.

As the experiments are usually performed on a very large graphene system with a specific impurity distribution, we also investigate the electron transport along a single disordered, larger GNR sample. Figure 2(a) shows the energy-dependent conductance G of a single disordered GNR with $M = 10^4$ and 10^5, while Fig. 2(b) displays the magnified view in the green rectangle of Fig. 2(a). One can see from Fig. 2(a) that the conductance is finite and oscillates considerably around each QCP position due to the quantum coherence. Although the overall conductance is declined by increasing M, the QCPs of conductance quantum remain at a narrow but continuous energy region for such a long GNR of $M = 10^5$, as illustrated in Fig. 2(b).

IV. WIDTH-DEPENDENT QCPs

We then study the electron transport through disordered GNRs by considering the nanoribbon width, as shown in Fig. 3(a), where $\langle G \rangle$ vs E is displayed for typical values of N. One can see that the number of QCPs increases with N, owing to the increment of transport modes. Further studies indicate that the number of all QCPs found in the whole energy spectrum is $\lfloor N/2 \rfloor$ for disordered GNRs of width N, with $\lfloor \cdots \rfloor$ the floor function, as can be seen from Table II. Some QCPs for $N = 39$ overlap all those for $N = 19$, while the remaining QCPs overlap all those for $N = 20$ by properly shifting their positions. Interestingly, the two QCPs locate at the same energies for $N = 9$, 19, and 39 [see the stars in Fig. 3(a)]. This phenomenon can also be detected in other disordered GNRs with various widths, as shown in Fig. 3(b), where the evolution of all the QCPs in the energy region $[-t, t]$ is displayed by ranging the width from $N = 3$ to 40. For example, identical QCPs are observed at $E \sim -0.618t$ for $N = 4$, 9, 14, . . ., at $E \sim 0$ for $N = 5$, 8, 11, . . ., and at
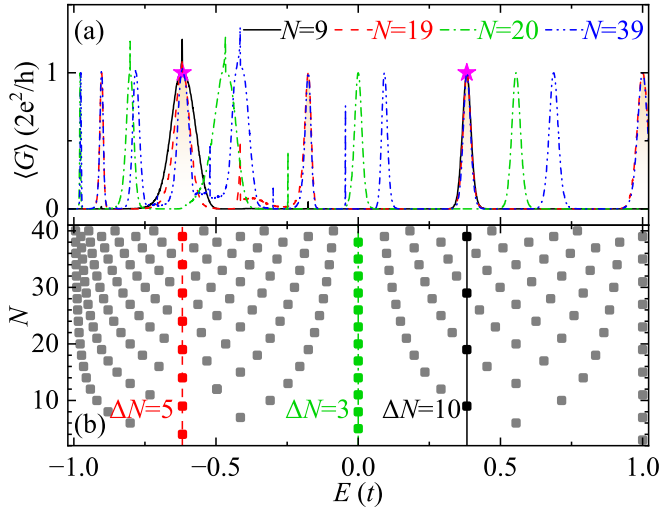
FIG. 3. Electron transport along disordered armchair GNRs with different widths. (a) Energy-dependent $\langle G \rangle$ for different widths N. (b) Evolution of the QCPs for different N. Here, $n_a = 50\%$ and the other parameters are the same as in Fig. 1(c).

$E \sim 0.382t$ for $N = 9, 19, 29, \ldots$ [see the red dashed, green dashed-dotted, and black solid lines in Fig. 3(b)]. This evolution phenomenon can be formulated in an arithmetic sequence of $N_j = j\Delta N - 1$, with j an integer and ΔN the width difference between two successive disordered GNRs of identical QCPs.

V. PHYSICAL ORIGIN OF QCPs

To understand the width-dependent QCPs, Figs. 4(a) and 4(b) show the distributions of bond currents for two disordered GNR samples at the two QCP positions marked by the stars in Fig. 3(a), which can be calculated from the lesser Green's function [79–82]. Here, the arrow size is proportional to the magnitude of bond currents. One can see that the currents only flow along the bonds between neighboring carbon atoms, and thus the scattering from the adatoms disappears, leading to the emergence of the QCPs. Furthermore, one can identify other important features from Fig. 4, which hold for all the investigated disordered GNRs of various adatom distributions. (i) The spatial mirror symmetry is maintained with respect to the $(N + 1)/2$ row for odd N. (ii) The fifth row for $N = 9$ and the tenth row for $N = 19$, where the bond currents are zero, can be used to divide each disordered GNR into two isolated segments with identical distributions of bond currents. As a

TABLE I. Sum of the wave function of the six carbon atoms in every hexagon at different momenta k_x, as marked by the magenta diamonds in Fig. 5(b).

	$E \sim -0.618t$		$E \sim 0.382t$	
	$k_x = -0.4\pi$	$k_x = -0.352\pi$	$k_x = 0.2\pi$	$k_x = 0.004\pi$
I	0	$0.255 - 0.256i$	0	$0.000 - 0.003i$
II	0	$-0.158 + 0.158i$	0	$0.000 + 0.005i$
III	0	$-0.158 + 0.158i$	0	$0.000 - 0.005i$
IV	0	$0.255 - 0.256i$	0	$0.000 + 0.003i$
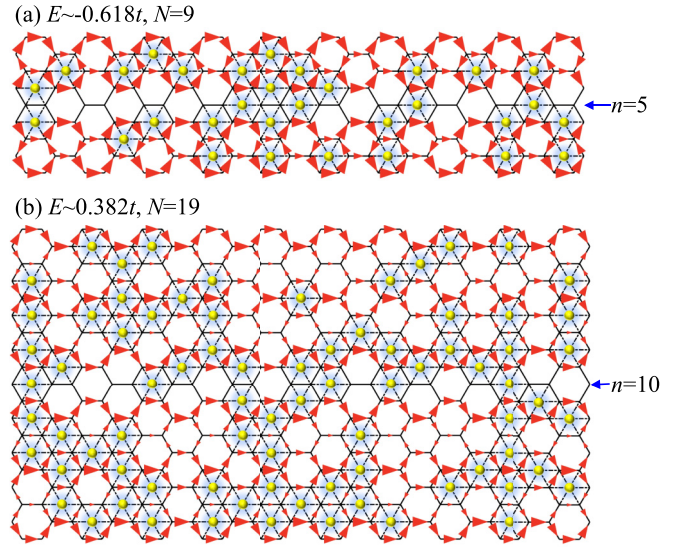
FIG. 4. Spatial distributions of bond currents of two individual disordered GNR samples for the QCPs at (a) $E \sim -0.618t$ with $N = 9$ and (b) $E \sim 0.382t$ with $N = 19$, as marked by the stars in Fig. 3(a). The two panels refer to the middle segment of disordered GNRs with $M = 2 \times 10^4 + 20$, and the arrow size is proportional to the magnitude of bond currents.

result, identical QCPs can be observed at $E \sim -0.618t$ for $N_j = 4$ and 9, and at $E \sim 0.382t$ for $N_j = 9$ and 19. We conclude that, by applying the zero-current row to divide the disordered GNR into the smallest segment, the width at which the quantized perfect transmission happens with identical QCPs can be determined.

To further elucidate the physical origin of the QCPs, we calculate the wave function of specific electronic states at which the QCPs take place. Figures 5(a) and 5(b) plot, respectively, the unit cell and the dispersion relation of the pristine GNR with $N = 9$. Here, the carbon atoms and hexagons are labeled by arabic and roman numerals, respectively. The blue dashed-dotted and dashed lines correspond to the QCP positions [see the stars in Fig. 3(a)], and these two lines independently intersect the dispersion relation, as shown by the magenta diamonds and the inset in Fig. 5(b). Table I displays the sum of the wave function of the six carbon atoms in every
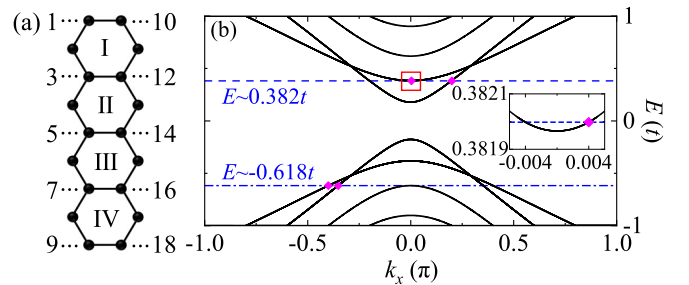
FIG. 5. (a) Unit cell and (b) dispersion relation of armchair GNR with $N = 9$. The carbon atoms and hexagons in (a) are described by the arabic and roman numerals, respectively. The magenta diamonds in (b) refer to specific momenta at which energies the QCPs take place, as marked by the stars in Fig. 3(a).

TABLE II. Momenta k_x and the corresponding QCP energies of various GNRs with width ranging from $N = 3$ to 20, at which the sum of the wave function of the six carbon atoms in every hexagon is zero.

N	E (t)	k_x (π)	N	E (t)	k_x (π)	N	E (t)	k_x (π)	N	E (t)	k_x (π)
3	1	$\frac{2}{4}(\frac{1}{2})$	11	-0.732	$\frac{-6}{12}(\frac{-1}{2})$	15	-0.8478	$\frac{-10}{16}(\frac{-5}{8})$	18	-0.9727	$\frac{-16}{19}$
4	-0.618	$\frac{-2}{5}$	11	0	$\frac{0}{12}(0)$	15	-0.4142	$\frac{-4}{16}(\frac{-1}{4})$	18	-0.7589	$\frac{-10}{19}$
4	1.618	$\frac{4}{5}$	11	1	$\frac{6}{12}(\frac{1}{2})$	15	0.2347	$\frac{2}{16}(\frac{1}{8})$	18	-0.3547	$\frac{-4}{19}$
5	0	$\frac{0}{6}(0)$	11	2	$\frac{12}{12}(1)$	15	1	$\frac{8}{16}(\frac{1}{2})$	18	0.1966	$\frac{2}{19}$
5	2	$\frac{6}{6}(1)$	11	2.732	$\frac{18}{12}(\frac{3}{2})$	15	1.765	$\frac{14}{16}(\frac{7}{8})$	18	0.8348	$\frac{8}{19}$
6	-0.8019	$\frac{-4}{7}$	12	-0.9419	$\frac{-10}{13}$	15	2.4142	$\frac{20}{16}(\frac{5}{4})$	18	1.491	$\frac{14}{19}$
6	0.5551	$\frac{2}{7}$	12	-0.497	$\frac{-4}{13}$	15	2.8478	$\frac{26}{16}(\frac{13}{8})$	18	2.094	$\frac{20}{19}$
6	2.247	$\frac{8}{7}$	12	0.2908	$\frac{2}{13}$	16	-0.966	$\frac{-14}{17}$	18	2.578	$\frac{26}{19}$
7	-0.4142	$\frac{-2}{8}(\frac{-1}{4})$	12	1.242	$\frac{8}{13}$	16	-0.7005	$\frac{-8}{17}$	18	2.891	$\frac{32}{19}$
7	1	$\frac{4}{8}(\frac{1}{2})$	12	2.1361	$\frac{14}{13}$	16	-0.2053	$\frac{-2}{17}$	19	-0.9021	$\frac{-14}{20}(\frac{-7}{10})$
7	2.4142	$\frac{10}{8}(\frac{5}{4})$	12	2.7709	$\frac{20}{13}$	16	0.4527	$\frac{4}{17}$	19	-0.618	$\frac{-8}{20}(\frac{-2}{5})$
8	-0.879	$\frac{-6}{9}(\frac{-2}{3})$	13	-0.8019	$\frac{-8}{14}(\frac{-4}{7})$	16	1.184	$\frac{10}{17}$	19	-0.1756	$\frac{-2}{20}(\frac{-1}{10})$
8	0	$\frac{0}{9}(0)$	13	-0.247	$\frac{-2}{14}(\frac{-1}{7})$	16	1.891	$\frac{16}{17}$	19	0.3819	$\frac{4}{20}(\frac{1}{5})$
8	1.347	$\frac{6}{9}(\frac{2}{3})$	13	0.555	$\frac{4}{14}(\frac{2}{7})$	16	2.478	$\frac{22}{17}$	19	1	$\frac{10}{20}(\frac{1}{2})$
8	2.532	$\frac{12}{9}(\frac{4}{3})$	13	1.445	$\frac{10}{14}(\frac{5}{7})$	16	2.864	$\frac{28}{17}$	19	1.618	$\frac{16}{20}(\frac{4}{5})$
9	-0.618	$\frac{-4}{10}(\frac{-2}{5})$	13	2.247	$\frac{16}{14}(\frac{8}{7})$	17	-0.8794	$\frac{-12}{18}(\frac{-2}{3})$	19	2.176	$\frac{22}{20}(\frac{11}{10})$
9	0.382	$\frac{2}{10}(\frac{1}{5})$	13	2.801	$\frac{22}{14}(\frac{11}{7})$	17	-0.5321	$\frac{-6}{18}(\frac{-1}{3})$	19	2.618	$\frac{28}{20}(\frac{7}{5})$
9	1.618	$\frac{8}{10}(\frac{4}{5})$	14	-0.956	$\frac{-12}{15}(\frac{-4}{5})$	17	0	$\frac{0}{18}(0)$	19	2.902	$\frac{34}{20}(\frac{17}{10})$
9	2.618	$\frac{14}{10}(\frac{7}{5})$	14	-0.618	$\frac{-6}{15}(\frac{-2}{5})$	17	0.6527	$\frac{6}{18}(\frac{1}{3})$	20	-0.9777	$\frac{-18}{21}(\frac{-6}{7})$
10	-0.919	$\frac{-8}{11}$	14	0	$\frac{0}{15}(0)$	17	1.347	$\frac{12}{18}(\frac{2}{3})$	20	-0.8019	$\frac{-12}{21}(\frac{-4}{7})$
10	-0.3097	$\frac{-2}{11}$	14	0.791	$\frac{6}{15}(\frac{2}{5})$	17	2	$\frac{18}{18}(1)$	20	-0.4661	$\frac{-6}{21}(\frac{-2}{7})$
10	0.7153	$\frac{4}{11}$	14	1.618	$\frac{12}{15}(\frac{4}{5})$	17	2.532	$\frac{24}{18}(\frac{4}{3})$	20	0	$\frac{0}{21}(0)$
10	1.831	$\frac{10}{11}$	14	2.338	$\frac{18}{15}(\frac{6}{5})$	17	2.8794	$\frac{30}{18}(\frac{5}{3})$	20	0.555	$\frac{6}{21}(\frac{2}{7})$
10	2.681	$\frac{16}{11}$	14	2.827	$\frac{24}{15}(\frac{8}{5})$				20	1.1495	$\frac{12}{21}(\frac{4}{7})$
									20	1.731	$\frac{18}{21}(\frac{6}{7})$
									20	2.247	$\frac{24}{21}(\frac{8}{7})$
									20	2.652	$\frac{30}{21}(\frac{10}{7})$
									20	2.911	$\frac{36}{21}(\frac{12}{7})$

hexagon at different momenta k_x, where the wave function of all the carbon atoms is shown in Table S1 of the Supplemental Material [78]. We can see from Table I that, at the QCP positions, there always exists one specific momentum k_x, at which the sum of the wave function is exactly zero. We further calculate all these momenta k_x of various GNRs of different widths, as shown in Table II. Interestingly, one can infer from Table II that these momenta of GNRs equidistantly distribute within $[-\pi, 2\pi]$ and can be expressed as

$$k_x = \frac{6n - N + 2 + 3[1 - (-1)^N]/2}{N + 1}\pi, \qquad (2)$$

where $n = 0, 1, \ldots, \lfloor N/2 \rfloor - 1$. We then write down the Schrödinger equation on the carbon atoms,

$$E\psi_i = -t \sum_{\langle j \rangle_i} \psi_j + \sum_{\langle \alpha \rangle_i} \gamma_\alpha \varphi_\alpha, \qquad (3)$$

where ψ_i is the wave function of carbon atoms at position r_i, j is the site index for all the neighboring carbon atoms around site i, and α is the one for all the neighboring adatoms to i, with φ_α the wave function of adatoms. Similarly, for the

adatoms, we have $(E - \epsilon_\alpha)\varphi_\alpha = \gamma_\alpha \sum_{\langle j' \rangle_\alpha} \psi_{j'}$. Substituting φ_α into Eq. (3), we derive

$$E\psi_i = -t \sum_{\langle j \rangle_i} \psi_j + \sum_{\langle \alpha \rangle_i} \frac{\gamma_\alpha^2}{E - \epsilon_\alpha} \sum_{\langle j' \rangle_\alpha} \psi_{j'}. \qquad (4)$$

It can be deduced from Eq. (4) that if the sum of wave function $\psi_{j'}$ of the six carbon atoms around the adatom α equals zero, the second term on the right-hand side vanishes. This elucidates why the adatoms have no impact on the electron transport for this special transport mode, where the electrons propagate ballistically through disordered GNRs, leading to a single quantized conductance of $2e^2/h$, while for other transport modes, the presence of random adatoms significantly alters their behavior, causing the electrons to become Anderson localized. Consequently, a QCP of conductance quantum emerges. This phenomenon can find its analogy in disordered quantum Hall systems where only the dissipationless Hall edge states contribute to a quantized conductance [83–86], but the physical origin is different.

Finally, let us discuss how the QCPs could be realized in experiments. At first, pristine GNRs are prepared by, e.g.,

mechanical exfoliation or chemical vapor deposition, and are placed on an insulating layer. After that, heavy atoms, which preferentially adsorb at hollow sites of graphene, are ejected from a high-purity bulk sample with an *e*-beam evaporator, and they are then deposited onto the surface of pristine GNRs at low temperatures of ∼10 K [87,88]. Finally, the charge transport measurements are carried out at low temperatures.

VI. CONCLUSIONS

In summary, we investigate the electron transport through GNRs with random hollow adatoms. We uncover unexpected QCPs at specific energies within the transmission spectrum, alongside the overall suppression of conductance. These QCPs are found to be very robust against system size, GNR edge, and adatom properties, and most importantly, they can survive in the presence of Anderson localization. A system-

atic analysis on distributions of bond currents and the wave function reveals the ballistic transport feature of these exotic QCPs. Our findings contribute significantly to the understanding of the interplay between graphene and impurities, offering valuable insights for the design of conductance switches in graphene-based materials utilizing hollow adatoms.

ACKNOWLEDGMENTS

[1] A. Hashimoto, K. Suenaga, A. Gloter, K. Urita, and S. Iijima, Direct evidence for atomic defects in graphene layers, Nature (London) **430**, 870 (2004).

[2] S. Ihnatsenka and G. Kirczenow, Conductance quantization in strongly disordered graphene ribbons, Phys. Rev. B **80**, 201407(R) (2009).

[3] Q. Tang, Z. Zhou, and Z. Chen, Graphene-related nanomaterials: Tuning properties by functionalization, Nanoscale **5**, 4541 (2013).

[4] C. H. A. Wong, Z. Sofer, M. Kubešová, J. Kučera, S. Matějková, and M. Pumera, Synthetic routes contaminate graphene materials with a whole spectrum of unanticipated metallic elements, Proc. Natl. Acad. Sci. USA **111**, 13774 (2014).

[5] Y. Lum, Y. Kwon, P. Lobaccaro, L. Chen, E. L. Clark, A. T. Bell, and J. W. Ager, Trace levels of copper in carbon materials show significant electrochemical CO_2 reduction activity, ACS Catal. **6**, 202 (2016).

[6] R. Jalili, D. Esrafilzadeh, S. H. Aboutalebi, Y. M. Sabri, A. E. Kandjani, and S. K. Bhargava, Silicon as a ubiquitous contaminant in graphene derivatives with significant impact on device performance, Nat. Commun. **9**, 5070 (2018).

[7] K. R. Nandanapalli, D. Mudusu, and S. Lee, Functionalization of graphene layers and advancements in device applications, Carbon **152**, 954 (2019).

[8] L. Lin, J. Zhang, H. Su, J. Li, L. Sun, Z. Wang, F. Xu, C. Liu, S. Lopatin, Y. Zhu, K. Jia, S. Chen, D. Rui, J. Sun, R. Xue, P. Gao, N. Kang, Y. Han, H. Q. Xu, Y. Cao *et al.*, Towards super-clean graphene, Nat. Commun. **10**, 1912 (2019).

[9] F. Qing, Y. Zhang, Y. Niu, R. Stehle, Y. Chen, and X. Li, Towards large-scale graphene transfer, Nanoscale **12**, 10890 (2020).

[10] W. Du, H. Wu, H. Chen, G. Xu, and C. Li, Graphene oxide in aqueous and nonaqueous media: Dispersion behaviour and solution chemistry, Carbon **158**, 568 (2020).

[11] W. Kiciński and S. Dyjak, Transition metal impurities in carbon-based materials: Pitfalls, artifacts and deleterious effects, Carbon **168**, 748 (2020).

[12] M. I. Katsnelson, K. Novoselov, and A. K. Geim, Chiral tunnelling and the Klein paradox in graphene, Nat. Phys. **2**, 620 (2006).

[13] K. Wakabayashi, Y. Takane, and M. Sigrist, Perfectly conducting channel and universality crossover in disordered graphene nanoribbons, Phys. Rev. Lett. **99**, 036601 (2007).

[14] C. W. J. Beenakker, Colloquium: Andreev reflection and Klein tunneling in graphene, Rev. Mod. Phys. **80**, 1337 (2008).

[15] A. F. Young and P. Kim, Quantum interference and Klein tunnelling in graphene heterojunctions, Nat. Phys. **5**, 222 (2009).

[16] N. Stander, B. Huard, and D. Goldhaber-Gordon, Evidence for Klein tunneling in graphene *p-n* junctions, Phys. Rev. Lett. **102**, 026807 (2009).

[17] A. Rycerz, Random matrices and quantum chaos in weakly disordered graphene nanoflakes, Phys. Rev. B **85**, 245424 (2012).

[18] J. P. Robinson, H. Schomerus, L. Oroszlány, and V. I. Fal'ko, Adsorbate-limited conductivity of graphene, Phys. Rev. Lett. **101**, 196803 (2008).

[19] F. Gargiulo, G. Autès, N. Virk, S. Barthel, M. Rösner, L. R. M. Toller, T. O. Wehling, and O. V. Yazyev, Electronic transport in graphene with aggregated hydrogen adatoms, Phys. Rev. Lett. **113**, 246601 (2014).

[20] S. Gattenlöhner, W.-R. Hannes, P. M. Ostrovsky, I. V. Gornyi, A. D. Mirlin, and M. Titov, Quantum Hall criticality and localization in graphene with short-range impurities at the Dirac point, Phys. Rev. Lett. **112**, 026802 (2014).

[21] Y. G. Pogorelov, V. M. Loktev, and D. Kochan, Impurity resonance effects in graphene versus impurity location, concentration, and sublattice occupation, Phys. Rev. B **102**, 155414 (2020).

[22] Y. G. Pogorelov and V. M. Loktev, Impurity effects on Dirac modes in graphene armchair nanoribbons, Phys. Rev. B **106**, 224202 (2022).

[23] S. M. Kozlov, F. Viñes, and A. Görling, Bandgap engineering of graphene by physisorbed adsorbates, Adv. Mater. **23**, 2638 (2011).

[24] Z. Lin, W. Qin, J. Zeng, W. Chen, P. Cui, J.-H. Cho, Z. Qiao, and Z. Zhang, Competing gap opening mechanisms of monolayer graphene and graphene nanoribbons on strong topological insulators, Nano Lett. **17**, 4013 (2017).

[25] T. Terasawa, K. Matsunaga, N. Hayashi, T. Ito, S. I. Tanaka, S. Yasuda, and H. Asaoka, Band gap opening in graphene by

hybridization with Au (001) reconstructed surfaces, Phys. Rev. Mater. **7**, 014002 (2023).

[26] C. Cao, M. Wu, J. Jiang, and H.-P. Cheng, Transition metal adatom and dimer adsorbed on graphene: Induced magnetization and electronic structures, Phys. Rev. B **81**, 205424 (2010).

[27] T. O. Wehling, A. I. Lichtenstein, and M. I. Katsnelson, Transition-metal adatoms on graphene: Influence of local Coulomb interactions on chemical bonding and magnetic moments, Phys. Rev. B **84**, 235110 (2011).

[28] W. Hu, C. Wang, H. Tan, H. Duan, G. Li, N. Li, Q. Ji, Y. Lu, Y. Wang, Z. Sun, F. Hu, and W. Yan, Embedding atomic cobalt into graphene lattices to activate room-temperature ferromagnetism, Nat. Commun. **12**, 1854 (2021).

[29] O. Dyck, L. Zhang, M. Yoon, J. L. Swett, D. Hensley, C. Zhang, P. D. Rack, J. D. Fowlkes, A. R. Lupini, and S. Jesse, Doping transition-metal atoms in graphene for atomic-scale tailoring of electronic, magnetic, and quantum topological properties, Carbon **173**, 205 (2021).

[30] K. Hatsuda, H. Mine, T. Nakamura, J. Li, R. Wu, S. Katsumoto, and J. Haruyama, Evidence for a quantum spin Hall phase in graphene decorated with Bi_2Te_3 nanoparticles, Sci. Adv. **4**, eaau6915 (2018).

[31] K. T. Chan, J. B. Neaton, and M. L. Cohen, First-principles study of metal adatom adsorption on graphene, Phys. Rev. B **77**, 235430 (2008).

[32] H. Jiang, Z. H. Qiao, H. W. Liu, J. R. Shi, and Q. Niu, Stabilizing topological phases in graphene via random adsorption, Phys. Rev. Lett. **109**, 116803 (2012).

[33] M. Lorenzo, C. Escher, T. Latychevskaia, and H.-W. Fink, Metal adsorption and nucleation on free-standing graphene by low-energy electron point source microscopy, Nano Lett. **18**, 3421 (2018).

[34] S. Irmer, D. Kochan, J. Lee, and J. Fabian, Resonant scattering due to adatoms in graphene: Top, bridge, and hollow positions, Phys. Rev. B **97**, 075417 (2018).

[35] B. A. Barker, A. J. Bradley, M. M. Ugeda, S. Coh, A. Zettl, M. F. Crommie, S. G. Louie, and M. L. Cohen, Geometry and electronic structure of iridium adsorbed on graphene, Phys. Rev. B **99**, 075431 (2019).

[36] S. Karan, T. Frank, T. Preis, J. Eroms, J. Fabian, F. Evers, and J. Repp, Interplay of boundary states of graphene nanoribbons with a Kondo impurity, Phys. Rev. B **105**, 205410 (2022).

[37] J. M. García-Lastra, Strong dependence of band-gap opening at the Dirac point of graphene upon hydrogen adsorption periodicity, Phys. Rev. B **82**, 235418 (2010).

[38] D. A. Abanin, A. V. Shytov, and L. S. Levitov, Peierls-type instability and tunable band gap in functionalized graphene, Phys. Rev. Lett. **105**, 086802 (2010).

[39] F. Marsusi, N. D. Drummond, and M. J. Verstraete, The physics of single-side fluorination of graphene: DFT and DFT+U studies, Carbon **144**, 615 (2019).

[40] L. Chen, F. Ouyang, S. Ma, T.-F. Fang, A.-M. Guo, and Q.-F. Sun, Enhancement of electron transport and band gap opening in graphene induced by adsorbates, Phys. Rev. B **101**, 115417 (2020).

[41] P. O. Lehtinen, A. S. Foster, A. Ayuela, A. Krasheninnikov, K. Nordlund, and R. M. Nieminen, Magnetic properties and diffusion of adatoms on a graphene sheet, Phys. Rev. Lett. **91**, 017202 (2003).

[42] Y. G. Zhou, X. T. Zu, F. Gao, H. F. Lv, and H. Y. Xiao, Adsorption-induced magnetic properties and metallic behavior of graphene, Appl. Phys. Lett. **95**, 123119 (2009).

[43] J. Nokelainen, I. V. Rozhansky, B. Barbiellini, E. Lähderanta, and K. Pussi, Gate-tunable magnetism of C adatoms on graphene, Phys. Rev. B **99**, 035441 (2019).

[44] T. Eelbo, M. Waśniowska, M. Gyamfi, S. Forti, U. Starke, and R. Wiesendanger, Influence of the degree of decoupling of graphene on the properties of transition metal adatoms, Phys. Rev. B **87**, 205443 (2013).

[45] M. Manadé, F. Viñes, and F. Illas, Transition metal adatoms on graphene: A systematic density functional study, Carbon **95**, 525 (2015).

[46] I. Shtepliuk and R. Yakimova, Interaction of epitaxial graphene with heavy metals: Towards novel sensing platform, Nanotechnology **30**, 294002 (2019).

[47] T. Preis, S. Vrbica, J. Eroms, J. Repp, and J. M. van Ruitenbeek, Current-induced one-dimensional diffusion of Co adatoms on graphene nanoribbons, Nano Lett. **21**, 8794 (2021).

[48] D. Marchenko, A. Varykhalov, M. R. Scholz, G. Bihlmayer, E. I. Rashba, A. Rybkin, A. M. Shikin, and O. Rader, Giant Rashba splitting in graphene due to hybridization with gold, Nat. Commun. **3**, 1232 (2012).

[49] F. Sánchez-Ochoa, Spin-polarized resonant tunneling in antiferromagnetic heterojunctions of graphene nanoribbons with 3d adatoms, Phys. Rev. Appl. **18**, 054068 (2022).

[50] C. Weeks, J. Hu, J. Alicea, M. Franz, and R. Wu, Engineering a robust quantum spin Hall state in graphene via adatom deposition, Phys. Rev. X **1**, 021001 (2011).

[51] D. Van Tuan, J. M. Marmolejo-Tejada, X. Waintal, B. K. Nikolić, S. O. Valenzuela, and S. Roche, Spin Hall effect and origins of nonlocal resistance in adatom-decorated graphene, Phys. Rev. Lett. **117**, 176602 (2016).

[52] F. J. Santos, D. A. Bahamon, R. B. Muniz, K. McKenna, E. V. Castro, J. Lischner, and A. Ferreira, Impact of complex adatom-induced interactions on quantum spin Hall phases, Phys. Rev. B **98**, 081407(R) (2018).

[53] S.-J. Jhan, M.-C. Wang, and C.-R. Chang, Spin-dependent transport properties in heavy-metal adatom decorated graphene nanoribbons, Results Phys. **22**, 103949 (2021).

[54] J. Hu, J. Alicea, R. Wu, and M. Franz, Giant topological insulator gap in graphene with 5d adatoms, Phys. Rev. Lett. **109**, 266801 (2012).

[55] P.-H. Chang, M. S. Bahramy, N. Nagaosa, and B. K. Nikolić, Giant thermoelectric effect in graphene-based topological insulators with heavy adatoms and nanopores, Nano Lett. **14**, 3779 (2014).

[56] B. Uchoa and A. H. C. Neto, Superconducting states of pure and doped graphene, Phys. Rev. Lett. **98**, 146801 (2007).

[57] G. Profeta, M. Calandra, and F. Mauri, Phonon-mediated superconductivity in graphene by lithium deposition, Nat. Phys. **8**, 131 (2012).

[58] B. M. Ludbrook, G. Levy, P. Nigge, M. Zonno, M. Schneider, D. J. Dvorak, C. N. Veenstra, S. Zhdanovich, D. Wong, P. Dosanjh, C. Straßer, A. Stöhr, S. Forti, C. R. Ast, U. Starke, and A. Damascelli, Evidence for superconductivity in Li-decorated monolayer graphene, Proc. Natl. Acad. Sci. USA **112**, 11795 (2015).

[59] J.-J. Zheng and E. R. Margine, First-principles calculations of the superconducting properties in Li-decorated monolayer

graphene within the anisotropic Migdal-Eliashberg formalism, Phys. Rev. B **94**, 064509 (2016).

[60] *Electronic Transport in Mesoscopic Systems*, edited by S. Datta (Cambridge University Press, Cambridge, UK, 1995).

[61] F. Libisch, S. Rotter, and J. Burgdörfer, Coherent transport through graphene nanoribbons in the presence of edge disorder, New J. Phys. **14**, 123006 (2012).

[62] P.-J. Hu, J.-T. Ding, Z.-R. Liang, T.-F. Fang, A.-M. Guo, and Q.-F. Sun, Enhanced electron transport and self-similarity in quasiperiodic borophene nanoribbons with line defects, Nanoscale **15**, 10740 (2023).

[63] Y.-R. Ding, D.-H. Xu, and C.-Z. Chen, Disorder and quantum transport of the helical quantum Hall phase in graphene, Phys. Rev. B **108**, 125409 (2023).

[64] J.-Y. Fang, Y.-C. Zhuang, and Q.-F. Sun, Absence of edge states at armchair edges in inhomogeneously strained graphene under a pseudomagnetic field, Phys. Rev. B **109**, 045430 (2024).

[65] P.-J. Hu, Z.-R. Liang, J.-W. Sun, T.-F. Fang, A.-M. Guo, and Q.-F. Sun, Contact effects on electron transport along disordered borophene nanoribbons with line defects, Phys. Rev. B **109**, 165437 (2024).

[66] V. Sessi, S. Stepanow, A. N. Rudenko, S. Krotzky, K. Kern, F. Hiebel, P. Mallet, J.-Y. Veuillen, O. Šipr, J. Honolka, and N. B. Brookes, Single $3d$ transition metal atoms on multi-layer graphene systems: Electronic configurations, bonding mechanisms and role of the substrate, New J. Phys. **16**, 062001 (2014).

[67] F. Ellinger, C. Franchini, and V. Bellini, Magnetic $3d$ adatoms on free-standing and Ni(111)-supported graphene, Phys. Rev. Mater. **5**, 014406 (2021).

[68] J. P. Carbone, J. Bouaziz, G. Bihlmayer, and S. Blügel, Magnetic properties of $4f$ adatoms on graphene: Density functional theory investigations, Phys. Rev. B **108**, 174431 (2023).

[69] M. Wang, M. Huang, D. Luo, Y. Li, M. Choe, W. K. Seong, M. Kim, S. Jin, M. Wang, S. Chatterjee, Y. Kwon, Z. Lee, and R. S. Ruoff, Single-crystal, large-area, fold-free monolayer graphene, Nature (London) **596**, 519 (2021).

[70] B. Lyu, J. Chen, S. Lou, C. Li, L. Qiu, W. Ouyang, J. Xie, I. Mitchell, T. Wu, A. Deng, C. Hu, X. Zhou, P. Shen, S. Ma, Z. Wu, K. Watanabe, T. Taniguchi, X. Wang, Q. Liang, J. Jia *et al.*, Catalytic growth of ultralong graphene nanoribbons on insulating substrates, Adv. Mater. **34**, 2200956 (2022).

[71] B. Lyu, J. Chen, S. Wang, S. Lou, P. Shen, J. Xie, L. Qiu, I. Mitchell, C. Li, C. Hu, X. Zhou, K. Watanabe, T. Taniguchi, X. Wang, J. Jia, Q. Liang, G. Chen, T. Li, S. Wang, W. Ouyang *et al.*, Graphene nanoribbons grown in hBN stacks for high-performance electronics, Nature (London) **628**, 758 (2024).

[72] S.-J. Xiong and Y. Xiong, Anderson localization of electron states in graphene in different types of disorder, Phys. Rev. B **76**, 214204 (2007).

[73] M. Evaldsson, I. V. Zozoulenko, H. Xu, and T. Heinzel, Edge-disorder-induced Anderson localization and conduction gap in graphene nanoribbons, Phys. Rev. B **78**, 161407(R) (2008).

[74] M. Y. Han, J. C. Brant, and P. Kim, Electron transport in disordered graphene nanoribbons, Phys. Rev. Lett. **104**, 056801 (2010).

[75] H. Yang, J. Zeng, Y. Han, and Z. Qiao, Anderson localization induced by spin-flip disorder in large-Chern-number quantum anomalous Hall effect, Phys. Rev. B **104**, 115414 (2021).

[76] K.-K. Bai, Y.-C. Wei, J.-B. Qiao, S.-Y. Li, L.-J. Yin, W. Yan, J.-C. Nie, and L. He, Detecting giant electron-hole asymmetry in graphene monolayer generated by strain and charge-defect scattering via Landau level spectroscopy, Phys. Rev. B **92**, 121405(R) (2015).

[77] Y. Zhang, Q. Q. Guo, S. Y. Li, and L. He, Nanoscale probing of broken-symmetry states in graphene induced by individual atomic impurities, Phys. Rev. B **101**, 155424 (2020).

[78] See Supplemental Material at http://link.aps.org/supplemental/10.1103/PhysRevB.110.064201 for (a) electron transport along disordered zigzag graphene nanoribbons with random hollow adsorbates and (b) wave function of all the carbon atoms at the QCPs.

[79] H. Jiang, L. Wang, Q.-F. Sun, and X. C. Xie, Numerical study of the topological Anderson insulator in HgTe/CdTe quantum wells, Phys. Rev. B **80**, 165316 (2009).

[80] C. H. Lewenkopf and E. R. Mucciolo, The recursive Green's function method for graphene, J. Comput. Electron. **12**, 203 (2013).

[81] P.-J. Hu, T.-F. Fang, A.-M. Guo, and Q.-F. Sun, Aharonov-Bohm-like effects and Fano resonances in circular DNA molecular junctions, Appl. Phys. Lett. **121**, 154102 (2022).

[82] The local current flowing from the mth slice to the $(m+1)$th one can be written as $\mathbf{I}_m = (-2e/h) \int [\mathbf{H}_{m,m+1} \mathbf{G}^<_{m+1,m}(\xi) - \mathbf{H}_{m+1,m} \mathbf{G}^<_{m,m+1}(\xi)] d\xi$. Here, $\mathbf{H}_{m+1,m}$ is the coupling matrix between the mth slice and the $(m+1)$th one, and $\mathbf{G}^<_{m,m+1}$ is the interchain lesser Green's function.

[83] B. Huckestein, Scaling theory of the integer quantum Hall effect, Rev. Mod. Phys. **67**, 357 (1995).

[84] L. Brey and H. A. Fertig, Edge states and the quantized Hall effect in graphene, Phys. Rev. B **73**, 195408 (2006).

[85] F. Duerr, J. B. Oostinga, C. Gould, and L. W. Molenkamp, Edge state transport through disordered graphene nanoribbons in the quantum Hall regime, Phys. Rev. B **86**, 081410(R) (2012).

[86] S. Kim, J. Schwenk, D. Walkup, Y. H. Zeng, F. Ghaharim, S. T. Le, M. R. Slot, J. Berwanger, S. R. Blankenship, K. Watanabe, T. Taniguchi, F. J. Ciessibl, N. B. Zhirenev, C. R. Dean, and J. A. Stroscio, Edge channels of broken-symmetry quantum Hall states in graphene visualized by atomic force microscopy, Nat. Commun. **12**, 2852 (2021).

[87] V. W. Brar, R. Decker, H.-M. Solowan, Y. Wang, L. Maserati, K. T. Chan, H. Lee, Ç. O. Girit, A. Zettl, S. G. Louie, M. L. Cohen, and M. F. Crommie, Gate-controlled ionization and screening of cobalt adatoms on a graphene surface, Nat. Phys. **7**, 43 (2011).

[88] F. Donati, Q. Dubout, G. Autès, F. Patthey, F. Calleja, P. Gambardella, O. V. Yazyev, and H. Brune, Magnetic moment and anisotropy of individual Co atoms on graphene, Phys. Rev. Lett. **111**, 236801 (2013).